ECS Transactions, 49 (1) 307-314 (2012)
10.1149/04901.0307ecst ©The Electrochemical Society

Influence of Silicon Binding Energy on Photoluminescence of Si-implanted Silicon Dioxide

A. A. González-Fernández[a], J. Juvert[a], M. Aceves-Mijares[b], A. Llobera[a], C. Domínguez[a]

[a] IMB-CNM-CSIC, Campus UAB, 08193 Bellaterra, Spain.

[b] INAOE, dpt. of Electronics, PO box 51, Puebla, Pue. 72000, Mexico.

Studies of photo-luminescence (PL) and X-ray Photoelectron Spectroscopy (XPS) were performed to silicon-rich silicon dioxide films (SRO) fabricated by implantation of *Si* ions on SiO_2 deposited by plasma enhanced chemical vapor deposition (PECVD). Samples presented PL spectra formed by the contribution of two bands, respectively related to defects and quantum confinement (QC). The XPS results for the different samples presented significant differences in the density and types of Si-Si and Si-O bonds. A relation was observed between the types of *Si* bonds and the PL characteristics presented by the material, obtaining a modulation of the emission spectra trough the change of the implantation dose.

Introduction

The promising arrival of a photonic device, which can be completely silicon-based and fully compatible with complementary metal-oxide-semiconductor (CMOS) technology, has been held back due to the difficulties to properly understand the complex mechanisms taking place in the materials used for its fabrication. These are mainly nano-structured materials that take advantage of some quantum phenomena that allows Silicon become a direct-bandgap material. One of these materials is the Silicon-rich silicon dioxide (SRO), which stands out for its flexibility and the possibility to use several CMOS compatible techniques for its fabrication, such as plasma-enhanced chemical vapor deposition (PECVD)[1,2], low pressure chemical vapor deposition (LPCVD)[3] or ionic implantation of silicon dioxide[4].

Structural and luminescence studies have been performed to SRO during the past years, and it is now generally accepted that its luminescence is mainly due to defect-related radiative transitions, quantum confinement effects (QC), or a combination of both[4–9]. However, there are many factors that affect the emission in this material, and still much work is needed in order to identify the structural properties that deliver specific luminescence characteristics. The relation between the atomic and binding characteristics of the elements that compose the SRO, and the way it emits light, can help to determine the processes needed to obtain the luminescence, and which characteristics are the best for a specific application.

In this work, the results of Photo Luminescence (PL) and X-ray Photoelectron Spectroscopy (XPS) studies to SRO films fabricated by the implantation of Si ions into silicon dioxide films are presented. Two main components of the photoemission spectra were identified, and it is discussed the relation between these and the density of particular silicon bond types determined by the structural studies.

Experimental

The fabrication of SRO films started with the deposition of a 30 nm thick stoichiometric SiO_2 film by PECVD on p-type silicon substrates with (100) crystalline orientation. A N_4Si_3 film with thickness of 30 nm was deposited by LPCVD on top of the silicon dioxide as an implantation buffer. A two-step Si ions implantation was performed, the first step with an energy of 25 keV, and the second with 50 keV to obtain a better control of the implanted ions distribution in the material as verified by SRIM simulations[10]. The dose of each step of the implantation was divided in order to reach the total doses presented in table I. The samples were then annealed in N_2 atmosphere at 1100 for 240 min to induce Si agglomeration[2], and the nitride buffer was removed by wet etching.

The final thickness and refractive index of the samples (table I) was obtained by ellipsometry using a laser with emission wavelength of 632.8 nm at an incident angle of 70°. Photo luminescence studies were performed normally stimulating the samples with an He+Cd laser light at 325nm, and collecting the photo-emission placing an optical fiber at an angle of 45°connected to an Ocean Optics QE6500 spectrometer. Filters to eliminate the laser line in the detector, and lenses to optimize focus were placed in the proper position to improve detection. Once identified the best detection conditions, those were fixed to obtain all PL spectra, and external illumination was controlled to guarantee the comparability of all the results. All spectra were corrected to the sensitivity of the spectrometer.

To observe the structural characteristics of the devices, XPS studies were performed in the same spots in which PL spectra were obtained using a Thermo Scientific K-Alpha XPS equipment with a monochromatic Kα radiation source from Al to 1486.68 eV, and an irradiation angle of 90° (normal to the sample). The pass energies used were 200 eV for full spectra and 50 eV for zone spectra. Depth profiles of XPS results (not shown) were obtained by the means of an Ar^+ sputtering gun under vacuum conditions (2.7×10^{-7} mbar) to avoid parasitic oxidation of the samples. These profiles confirmed that *Si* contents in the films was homogeneous from approximately 5nm below surface to 5nm above substrate, and a "flat zone" of each sample was defined as the zone in the layers cross-section within which the contents of Si, O and N did not varied significantly (less than 5%).

TABLE I. Implantation doses and final thicknesses and refractive indexes for the fabricated samples

Sample Label	Total dose (cm^{-2})	Final Thickness (nm)	Refractive index n
A	12×10^{16}	34±1	1.59±0.01
B	15×10^{16}	27±1	1.62±0.01
C	30×10^{16}	24±1	1.66±0.01

Results

The PL spectra of the samples are shown in figure 1. To rule out the influence of the thickness in the emission, the intensity was normalized to such value as obtained by ellipsometry in the area where PL was studied. Table I present the sample labels ant its respective thickness and refractive index values.

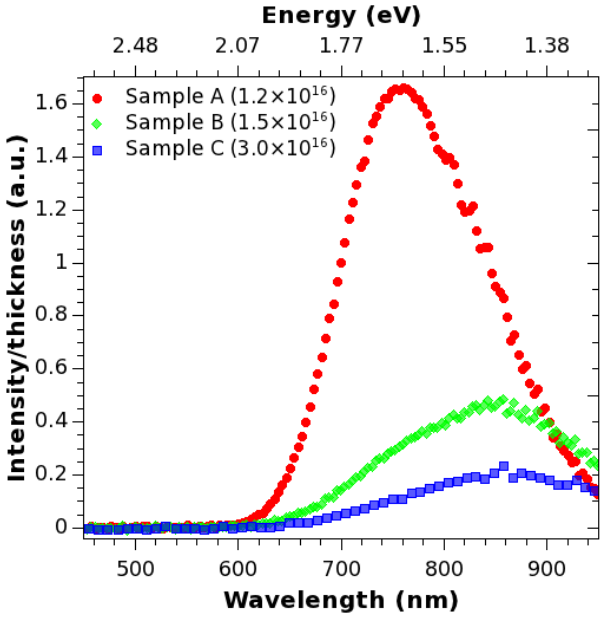

Figure 1. PL spectra for all samples. The intensity value in each measurement has been divided by the thickness of the respective layer in order to diminish its influence. All the measurements were performed under the same conditions.

It is clearly noticeable that the highest emission was observed in sample A, and the intensity decreased with the increment of the implantation dose. There is also a shift in both the maximum emission wavelength and spectrum shape. The reasons for this will be discussed in the following section.

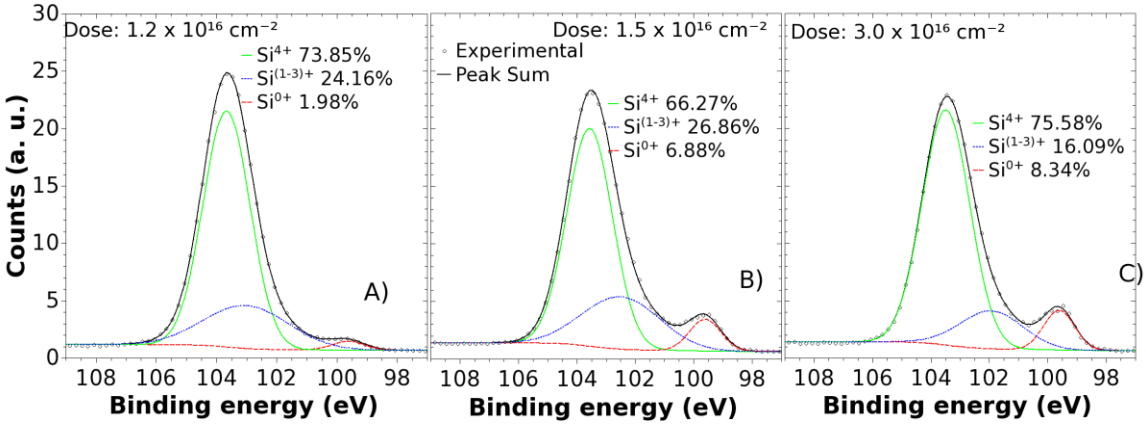

Figure 2: XPS spectra for the Si2p bonding region of all samples, bands that compose the spectra and relative contribution of such to full area.

In order to perform detailed studies of the Si2p bands, there were selected the results from the flat zone of the XPS profiles with the silicon contents values closest to the average. The Si2p spectra of all samples can be observed in figure 2. The experimental

data was fitted to a gaussian-lorentzian multi-peak function, in order to identify the five typical *Si* binding energies (the Si^{0+}, Si^{1+}, Si^{2+}, Si^{3+} and Si^{4+} found from 99 to 104eV[11]). The characteristic Si-Si binding energy from Si^{0+} (99.60±0.03 eV) was clearly identified, as well as the Si^{4+}, typically found in SiO_2 (103.50±0.10 eV). As for the rest of the Si binding energy peaks, it was decided to group them in a band with peak in the range 101.95-103.01 eV[12], which position varied from sample to sample. The area of this peak gives an idea of the compounds forming the interface between dioxide matrix and silicon nanoparticles in the frame of a core-shell model [8,12]. This band will be hereafter called $Si^{(1-3)+}$. Peaks within this region have been related to silicon sub nitrides and sub oxides[4], which is very consistent to the material under study.

TABLE II. Peak position and areas of the Gaussian components of PL spectra for all samples. Thickness is considered in all calculi.

Sample label	PL Band 1			PL Band 2		
	Peak position (nm)	Area (a. u.)	Contribution to PL (%)	Peak position (nm)	Area (a.u.)	Contribution to PL (%)
A	733±1	93.8±0.4	32.7±0.2	802±1	192.8±0.4	67.3±0.2
B	733±1	2.9±0.4	2.7±0.1	847±1	105.5±0.8	97.3±0.1
C	733±1	0.8±0.3	1.1±0.1	862±1	48.9±0.7	98.9±0.1

Discussion

Each PL spectrum was fitted to a two-Gaussian multi peak curve, reaching correlation factors higher than 99.8%. Figure 3 shows the components of the fitted curves, as well as the experimental points. The percentile contribution by each band to total PL can be observed in table II, and it is evident how the higher energy band (Band 1), decreases its contribution as compared to the lower energy band (Band 2) rather quickly as the Implantation dose increases. This decrement is noticeably pronounced, and gets up to a point in which Band 1 is almost neglected in total emission (Band 2 stands for more of the 97% and 98% of the photo-emission when the dose is 1.5×10^{16} cm^{-2} and 3×10^{16} cm^{-2}, respectively).

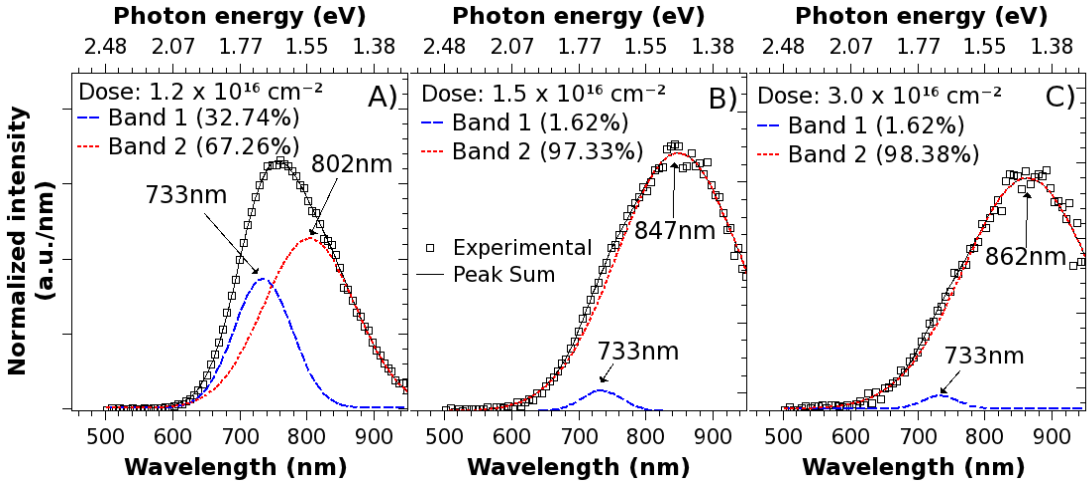

Figure 3. Multi-peak fittings of the PL spectra for each sample. Two Gaussian components were found in all samples. The highest energy one (Band 1) did not show a shift in maximum wavelength but only in maximum value, the lowest energy band (Band

2) changed both the maximum wavelength and intensity with different implantation doses.

Figure 4 shows the evolution of the center wavelength presented in table II. It can be observed how the position of the maximum emission wavelength of the Band 1 remains constant, while the Band 2 peak shifts towards lower energies as more Si is implanted into the films. This accounts for the significantly different shape of PL spectrum of sample A as compared to the other two.

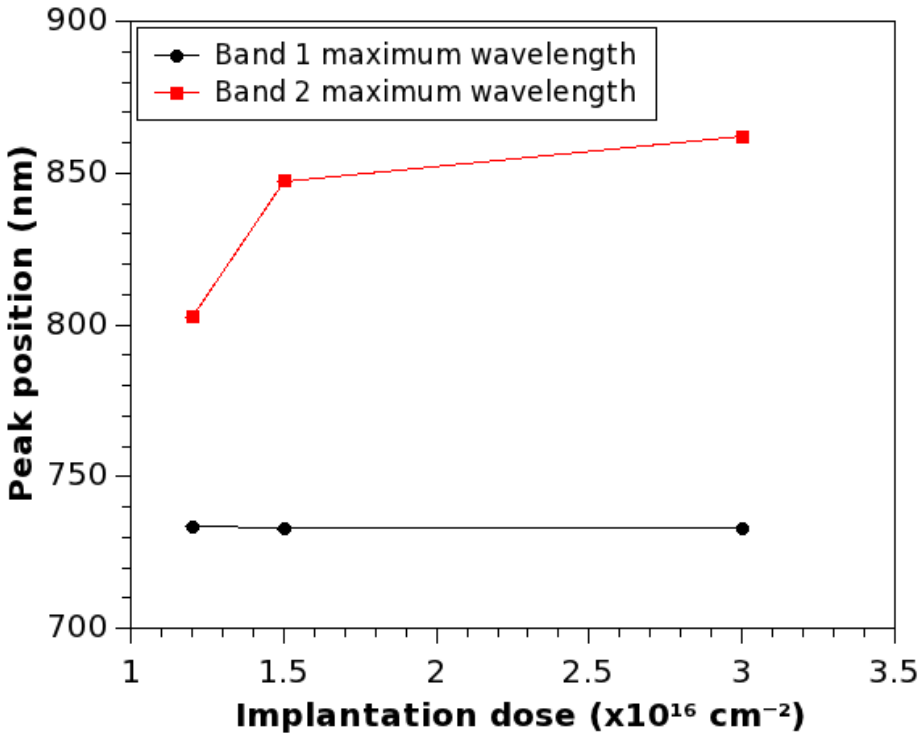

Figure 4. Position of peaks for Band 1 and Band 2 that compose the PL spectrum of samples as implantation dose is varied. Continuous lines are only eye guides.

The emission of Band 1 (peaking at 733±1nm, ~1.7eV) has been related to interactions taking place in the interface between the SiO_2 and silicon nano particles (Si-nps) of some silicon implanted oxides[4], and lower energy emission has been attributed to QC in such structures[1]. When analyzing XPS results, it can be seen how these two mechanisms are likely to be responsible for the respective PL bands.

The contribution to the total XPS spectrum area by each peak (Si^{0+}, $Si^{(1\text{-}3+)}$ and Si^{4+} presented in figure 2) is shown in figure 5. It can be seen how the contribution by the area of the Si^{0+}, hence the density of the corresponding *Si–Si* bonds, increments with the implantation dose. This is no surprise since after thermal annealing Si agglomeration is induced, and as the Si contents increases, more or bigger agglomerates are to be expected. However, the Si^{4+} and $Si^{(1\text{-}3)+}$ do not present a monotonous trend, as the SiO_2 bonds are less abundant in the second implantation than in the first, and then again

increases in the highest dose sample. Conversely, the $Si^{(1-3)+}$ peak presents quite an opposite behavior, diminishing from second to third implantation dose.

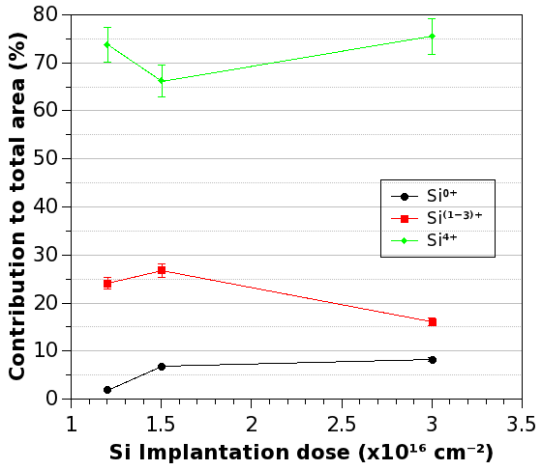

Figure 5. Contribution of the area of each peak to the total area as the implantation dose is increased. Solid lines are only eye guides.

Despite the larger area of the Si^{0+} Gaussian-Lorentzian peak in the XPS of the highest dose samples, it would be expected a more pronounced increment from second to third implantation, given the fact that the dose is doubled. However, there seems to be a saturation trend regarding the density of *Si*−*Si* bonds, and the evolution of the $Si^{(1-3)+}$ and Si^{4+} bands suggests that as more Si atoms are implanted into the material, there is a diminution of sub-stoichiometric oxides in favor of SiO_2, with less contribution of such atoms to the Si^{0+} bonds, causing the increment of the nano particles radii to slow its pace while the volume of the shell diminishes. This is confirmed by a shift of the $Si^{(1-3)+}$ peak towards the Si^{4+} value as dose increases (103, 102 and 101.95eV for samples A, B and C, respectively). Hence the material gets closer to a perfect SiO_2 matrix embedding Si-nps with slowly growing size as the silicon contents increases.

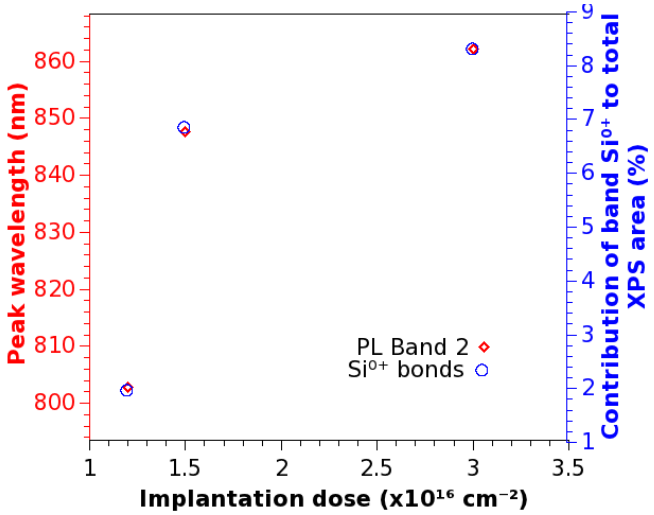

Figure 6: Evolution of the peak of the lower energy band part of PL (left vertical axis, rhombus) and contribution of the Si^{0+} Gaussian to the total area of the Si2p zone of XPS spectra (right vertical axis, circles) as the implantation dose of layers is increased.

This transit of the dielectric matrix towards a perfect silicon dioxide may account for one apparent inconsistency of the core shell model and the behavior of the Band 1emission: if it is accepted that defects are responsible for the Band 1 of PL, and that most defects should be located in the shells of the core-shell structure, then the behavior of this band appears not to be consistent to the evolution of the $Si^{(1-3)+}$ peak in XPS, which increases from sample A to B, while the contribution of defect-related to total PL drops from ~33% down to ~3%. It is possible that for contents of silicon below a certain value, the radiative defects are distributed along the SiO_2 matrix, and these are reduced when more Si atoms are implanted, remaining those in the shell.

Regarding the PL Band 2, it is consistent to QC as already mentioned, since the increment in the size/density of nano particles, indicated by the Si^{0+} band of XPS, is clearly related to the increment of this type of emission. Furthermore, the expected increment in the size of nps matches the shift towards lower wavelength emission found in PL Band 2 for higher implantation doses. This shift is remarkably consistent to *Si−Si* bond density, as can be observed in figure 6, in which the match between the area of the Si^{0+} peak, and the peak emission wavelength is almost perfect (note that proper limits for ordinate axis have been selected, but both are on linear scale).

This means that the photo emission wavelength of the SRO fabricated by implantation with this particular thermal treatment can be controlled by changing the implantation dose of the material, but such control can mainly be made by increasing or reducing the amount of *Si−Si* bonds in the material, since Band 1 (related to $Si^{(1-3)+}$ bonds) do not shows a change in peak, and its contribution to PL rapidly quenches as the *Si* contents is increased. On the other hand, the layers with the lowest relative contribution of Si^{0+} presented the greater PL intensity (see figure 3), and a compromise between intensity and control of emission wavelength should be considered when giving an specific application to the material.

Conclusion

The influence of implantation dose on PL and structural characteristics of II-SRO was studied, finding evidence of the presence of *Si−Si* particles embedded in SiO_2 with a shell of sub-stoichiometric oxide species in between. The volume of such shell, as related to thath of the Si-nps, presented a dependence on implantation dose. As the silicon implantation dose increases, the shell reduces its volume in favor of the creation of SiO_2 and *Si-Si* bonds, with a higher increase rate of the first kind. The PL was found to be composed by two main emission bands, one related to the shell and radiative defects, and the other to silicon nano particles and quantum confinement. The highest overall intensity was found in lower implantation dose samples, where defect-related band presented higher influence on PL. The emission wavelength of the defect-related band was independent of silicon contents, while QC-related light was highly dominant for implantation doses equal or higher than$1.5\times10^{16}cm^{-2}$. Hence, the emission wavelength can be controlled within a range by the variation of the size of the nanoparticles trough the implantation dose.

Acknowledgments

The authors acknowledge the grant received by CONACyT from México.

References

[1] Z. Ma, X. Liao, W. Cheng, J. He, *Status Solidi (b)* **1998**.

[2] M. Perálvarez, J. Barreto, J. Carreras, A. Morales, D. Navarro-Urrios, Y. Lebour, C. Domínguez, B. Garrido, *Nanotechnology* **2009**, *20*, 405201.

[3] A. Morales, J. Barreto, C. Dominguez, M. Riera, M. Aceves, J. Carrillo, *Physica E: Low-dimensional Systems and Nanostructures* **2007**, *38*, 54-58.

[4] T. Shimizu-Iwayama, N. Kurumado, D. Hole, *Journal of applied* **1998**, *83*, 6018-6022.

[5] G. Hadjisavvas, P. Kelires, *Physical Review Letters* **2004**, *93*, DOI 10.1103/PhysRevLett.93.226104.

[6] E. Lioudakis, A. Othonos, G. Hadjisavvas, P. Kelires, A. Nassiopoulou, *Physica E: Low-dimensional Systems and Nanostructures* **2007**, *38*, 128-134.

[7] S. Mirabella, R. Agosta, G. Franzò, I. Crupi, M. Miritello, R. Lo Savio, M. a. Di Stefano, S. Di Marco, F. Simone, A. Terrasi, *Journal of Applied Physics* **2009**, *106*, 103505.

[8] M. Ray, T. Basu, A. Jana, *Journal of Applied* **2010**, *107*, 064311.

[9] M. Ray, S. M. Hossain, R. F. Klie, K. Banerjee, S. Ghosh, *Nanotechnology* **2010**, *21*, 505602.

[10] J. Ziegler, *Nuclear Instruments and Methods in Physics Research Section B: Beam Interactions with Materials and Atoms* **2004**, *219-220*, 1027-1036.

[11] D.-Q. Yang, J.-N. Gillet, M. Meunier, E. Sacher, *Journal of Applied Physics* **2005**, *97*, 024303.

[12] S. Kim, M. C. Kim, S.-H. Choi, K. J. Kim, H. N. Hwang, C. C. Hwang, *Applied Physics Letters* **2007**, *91*, 103113.